Int. J. Electrochem. Sci., 15 **(2020)** 9611 – 9621, doi: 10.0964/2020.10.73

International Journal of ELECTROCHEMICAL SCIENCE
www.electrochemsci.org

Calcium Phosphate-Chitosan Coatings Deposited on Titanium Surfaces via Pulse Galvanostatic Electrodeposition for Dental Implants

Kyung Hee Park, Ho-Jun Song and Yeong-Joon Park[*]

Department of Dental Materials and Hard-tissue Biointerface Research Center, School of Dentistry, Chonnam National University, Gwangju 61186, Korea
[*]E-mail: yjpark@jnu.ac.kr

Received: 28 April 2020 / *Accepted:* 14 August 2020 / *Published:* 31 August 2020

Calcium phosphate/chitosan coatings were grown with various concentrations of chitosan solution by pulse electrodeposition. The coatings were deposited by 10 cycles of 5% to 20% chitosan by volume in deposition electrolyte. A uniform coating of calcium phosphate was deposited on a titanium surface and the underlying coating mechanism was investigated. The coatings were characterized by X-ray diffraction and scanning electron microscopy. The X-ray diffraction patterns and Fourier-transform infrared spectroscopy spectra confirmed the formation of dicalcium phosphate dihydrate and hydroxyl apatite. During electrodeposition, the reaction between calcium ions and reduced phosphate ions resulted in the formation of dicalcium phosphate dihydrate, which was converted to hydroxyl apatite. Homogenous spindle-like deposits were formed with controlled chitosan contents. The calcium phosphate/chitosan coatings acted as protective layers during electrodeposition. The control of chemical composition in the coatings affected corrosion behavior.

Keywords: Mineralization, Chitosan, Pulse electrodeposition, Calcium phosphate, Ccorrosion resistance

1. INTRODUCTION

Titanium and its alloys are commonly used in dental implants owing to their excellent mechanical and biological properties; however, they show poor chemical bonding with osseous structures. Several methods of depositing calcium phosphate (CaP) coatings on titanium substrates to enhance their surface bioactivity have been reported [1]. Calcium phosphates are biocompatible and speed up the bone growth on the surface of an implant during the early stages after implantation [2-4]. CaP are often nanocrystals that precipitate at room temperature [5]. However, their poor coating-to-substrate bond strength is not

favorable for bone repair [6]. Electrochemical deposition (ECD) facilitates calcium phosphate coating on metal substrates with complex shapes, such as dental implants and orthopedic fixation devices [7-9]. The advantage of electrodeposited CaP coating is easy control of the coating composition, which can be changed by adjusting the electrodeposition conditions [10, 11]. The different types of CaP coating developed via ECD include dicalcium phosphate dihydrate (DCPD, $CaHPO_4{\cdot}2H_2O$) [12], octacalcium phosphate (OCP, $Ca_8(HPO_4)_2(PO_4)_4{\cdot}5H_2O$) [13], and hydroxyapatite (HA, $Ca_{10}(OH)_2(PO_4)_6$) [14]. Recently, there has been a trend towards development of CaP/organic materials composite coatings, such as CaP/alginate and CaP/collagen on titanium, in order to produce new types of highly biocompatible and bioactive coatings [15, 16].

CaP/chitosan coatings have also attracted a good deal of research interest [17]. Chitosan is a natural polycationic liner polysaccharide prepared by deacetylation of chitin. It exhibits antimicrobial activity, good chemical stability, biocompatibility, biodegradability, and other properties conducive to biomedical implantation [18]. CaP/CS composites can be used to overcome the brittleness of CaP. CaP/chitosan composites have also been studied as bone substitutes, tissue engineering scaffolds, and bone cements. Park et al. reported that the preparation and properties of the CaP/chitosan composite formed by pulse deposition. However, according to the cycle number used for deposition, the CaP/chitosan composite showed a needle or network structure that was not similar among the composites. Also, it was difficult to control the thickness of the film [19]. Several researchers referred that potentiostatic deposition can be hard to control because a higher fraction of the applied potential is dropped across the irregular-shaped Ca-P deposits. Galvanostatic approaches with controlled current density can be easy setting their potentiostatic counterparts [20, 21]. Redepenning et al. generated chitosan/HA composite coatings using ECD by adding chitosan solution into the electrolyte. Pulse electrodeposition (PED) is used to make nano-deposits by adjusting the applied current and potential [22]. When the PED method is used, a large amount of hydrogen gas is generated, by which remarkably prevent nucleation and growth of CaP on the surface, resulting in porous and poorly attached coatings. The relaxation time between the two deposition times (pulse cycle) strongly reduces the emission of hydrogen gas and facilitates the diffusion of ions from the solution to the coating surface during PED. ECD was used to effectively functionalize porous titanium structures with CaP layers and increase controllability and reproducibility of the surface coating. However, few studies have been reported about the effects of CS content in electrolyte on the morphology and structure of CaP/CS coatings.

The aim of this study was to investigate the effects of electrodeposition parameters on coating morphology. The electrochemical properties of the CaP/CS coating and the structural properties of implant materials with the addition of chitosan to the deposition electrolyte were evaluated.

2. EXPERIMENTAL

2.1. Materials

Disks of commercially pure titanium (cp-Ti), each measuring 14 mm in diameter and 1.0 mm in thickness, were used as substrates for PED. These substrates were polished using different grades of SiC

paper (800 - 2000 grit), followed by washing with deionized water and ultrasonic cleansing with acetone, ethanol, and deionized water, and then dried under atmospheric conditions. Chitosan flake (CS, Sehwa Company, Korea) with 85% deacetylation and a molecular weight of about 520,000 g mol^{-1} was used. A 1% (w/v) CS aqueous solution was prepared by dissolving chitosan flake in 2% (v/v) acetic acid solution with stirring for 5 h.

2.2. Electrodeposition of CaP/CS coating

The deposition solution comprised 0.042 M $Ca(NO_3)_2 \cdot 4H_2O$ and 0.025 M $NaH_2PO_4 \cdot 4H_2O$ for a Ca/P ratio of 1.67 in distilled water. Electrolyte conductivity was improved by adding 0.1 M $NaNO_3$. The pH of the solution was adjusted to 4.3 at room temperature. Various amounts of CS solution, ranging from 5 to 20 v%, were added to the deposition electrolyte. Pulse amperometric deposition was carried out using a potentiostat (SP1, Wonatech, Korea). PED was conducted at a current density of – 5 mA cm^{-2} and a duty cycle of 0.5 at 37°C. A schematic of the electrochemical deposition setup is presented in Fig. 1. Electrodeposition of the CaP/CS coating was carried out in a typical two-electrode system. The cp-Ti substrate was used as the working electrode and acted as a cathode during the process. A Pt wire was used as the anode. The duty cycle is described as $t_{on}/(t_{on}+t_{off})$, in which t_{on} denotes the amount of time for which the current (– 5 mA cm^{-2}) was applied and t_{off} is the amount of time for which the set current (0 mA cm^{-2}) was applied. To maintain a uniform electrolyte concentration, the solution was stirred with a magnetic stirrer at a speed of 180 rpm. After PED, the coated substrates were rinsed with distilled water and dried at room temperature in air.

2.3. Characterization of the coatings

Scanning electron microscopy (SEM, Hitachi S4700) and energy dispersive X-ray spectroscopy (EDX, EMAX-7000, Horiba) were used to determine the surface morphology and elemental analysis of the coating. The coating structures were analyzed using an X-ray diffractometer (XRD model Philips X′pert) in the 2θ range of 5 - 70°. Fourier-transform infrared spectroscopy of the samples was done using an FT-IR spectrometer (Nicolet 380, Perkin Elmer, USA) over the frequency range of 400 – 4000 cm^{-1} with a spectral resolution of 2 cm^{-1}. Electrochemical studies were performed using a classical three-electrode cell. A Pt wire and a saturated calomel electrode (SCE) were used as the counter electrode and reference electrode, respectively. The working electrode was the CaP/CS coating samples on cp-Ti substrate. Potentiodynamic polarization studies were conducted in a potential range of – 2 to 1.0 V vs. SCE at a scan rate of 1 mV s^{-1}.

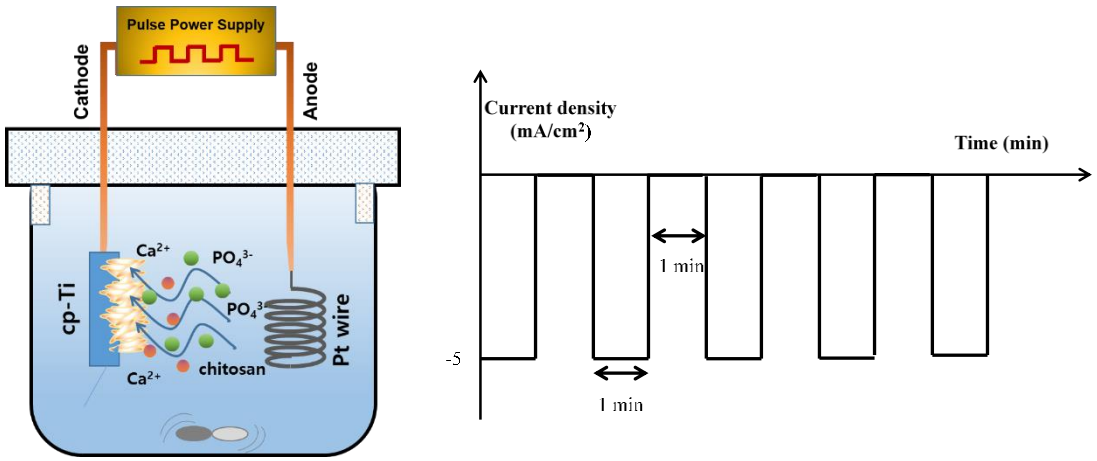

Figure 1. Schematic representation of the pulsed electrodeposition setup used for CaP/CS coating.

Electrochemical impedance spectroscopy (EIS) measurements were carried out in the frequency range from 10^5 Hz to 1 Hz with a signal amplitude of 5 mV. The equivalent circuit model for the measured impedance spectra were analyzed using Zman fitting software.

3. RESULTS AND DISCUSSION

Figure 2 shows SEM images of electrodeposited CaP/CS coatings at an applied current of -5 mA cm^{-2} with various concentrations of CS in the deposition electrolyte. As shown in Fig. 2(a), in the absence of chitosan in the deposition electrolyte, a dense and uniform coating of rod-like crystals was formed on the cp-Ti layer that covered the entire surface. All of the coatings made with 5 - 10 v% chitosan consisted of a compact network of fine spindles, as shown in Figure 2 (b-c). The 15 v% CaP/CS coating exhibited an aggregated spindle-like shape, which was highly aggregated in the CaP/CS coating when the chitosan content was increased to 20 v%. As the CS content increased, CaP crystals grew into a spindle-like morphology in the presence of 15 - 20 v% chitosan. The porous and spindle-like structure facilitated cell adsorption and growth. Multiple coating clusters also emerged from the dense layer adjacent to the substrate, which formed an extra layer. An increase in chitosan content of the deposition electrolyte resulted in grain formation on the coating surface. The grain formation occurred due to the generation of additional base following the addition of chitosan. The critical concentration of the Ca^{2+} and PO_4^{3-} facilitated agglomeration and grain formation. Furthermore, quantitative analysis of the X-ray spectrum showed that the Ca/P atomic ratios of the CaP/CS coatings were 1.0 to 1.2.

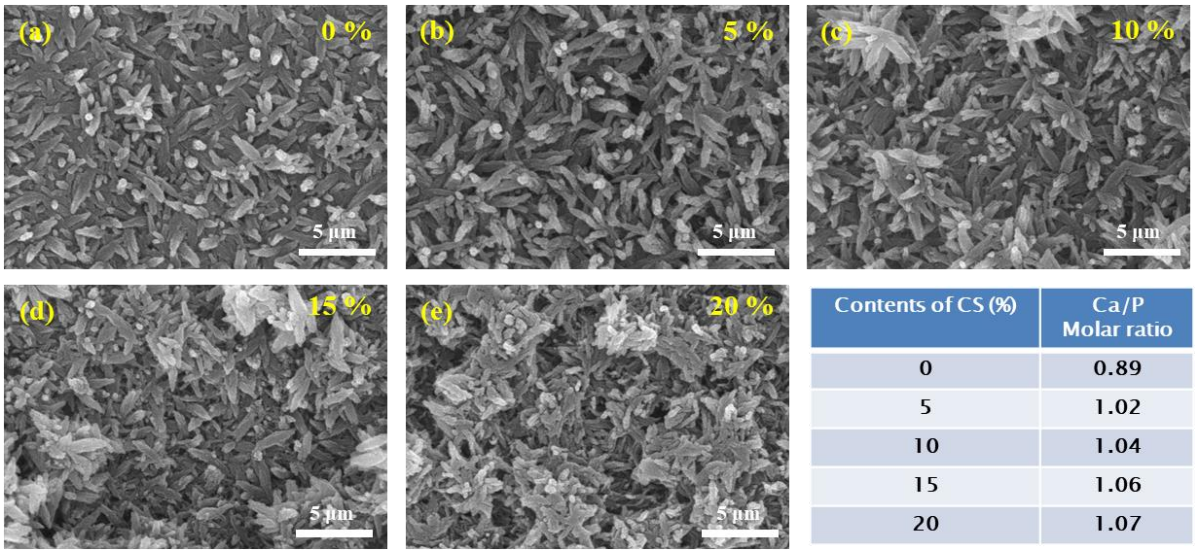

Contents of CS (%)	Ca/P Molar ratio
0	0.89
5	1.02
10	1.04
15	1.06
20	1.07

Figure 2. SEM images of calcium phosphate-chitosan coatings on a cp-Ti substrate created by 10 cycles of pulse amperometry at – 5 mA/cm^2 with different ratios of chitosan/calcium phosphate solution (0 - 20 v/v%).

The XRD patterns of the CaP/CS coating on the cp-Ti substrate are displayed in Fig. 3. The main XRD peaks corresponded to the (020), (021) and (041) crystallographic planes of DCPD (JCPDS 72-0713). The (002) and (211) diffraction peaks of hydroxyapatite (JCPDS 09-0432) at 2θ = 25.91° and 31.81°, respectively, appeared. The XRD results indicated that the as-deposited coating consisted of poorly crystalline DCPD and apatite. The formula for electrodeposition in an electrolyte containing chitosan is as follows [23]:

$$2H_2PO_4^- + 2e^- \rightarrow 2HPO_4^{2-} + H_2\uparrow \quad (1)$$

$$Ca^{2+} + HPO_4^{2-} + 2H_2O \rightarrow CaHPO_4{\cdot}2H_2O \quad (2)$$

As shown in Fig. 4, the FT-IR spectra of the CaP/CS coatings were obtained using different contents of chitosan solution. The band at 1037 cm^{-1} belong to asymmetric stretching vibration of PO_4^{3-}. The band at 607 and 561 cm^{-1} are due to PO_4^3 bending vibration. The band at 526 and 876 cm^{-1} correspond to the HPO_4^{2-}group [24]. The peak intensity of 20% CS was significantly higher than that of 5% - 15% CS, indicating that the 20% CS composite contained more PO_4^{3-} ions and a thicker coating than 5% - 15% CS. The characteristic group of CS, -NH_2, appears as a weak band at 1570 cm^{-1}, while the band of pure CS located at 1599 cm^{-1} [25]. The NH_2 peak of CaP/CS is blue-shifted from that of pure CS due to the bonding of N and Ca [26].

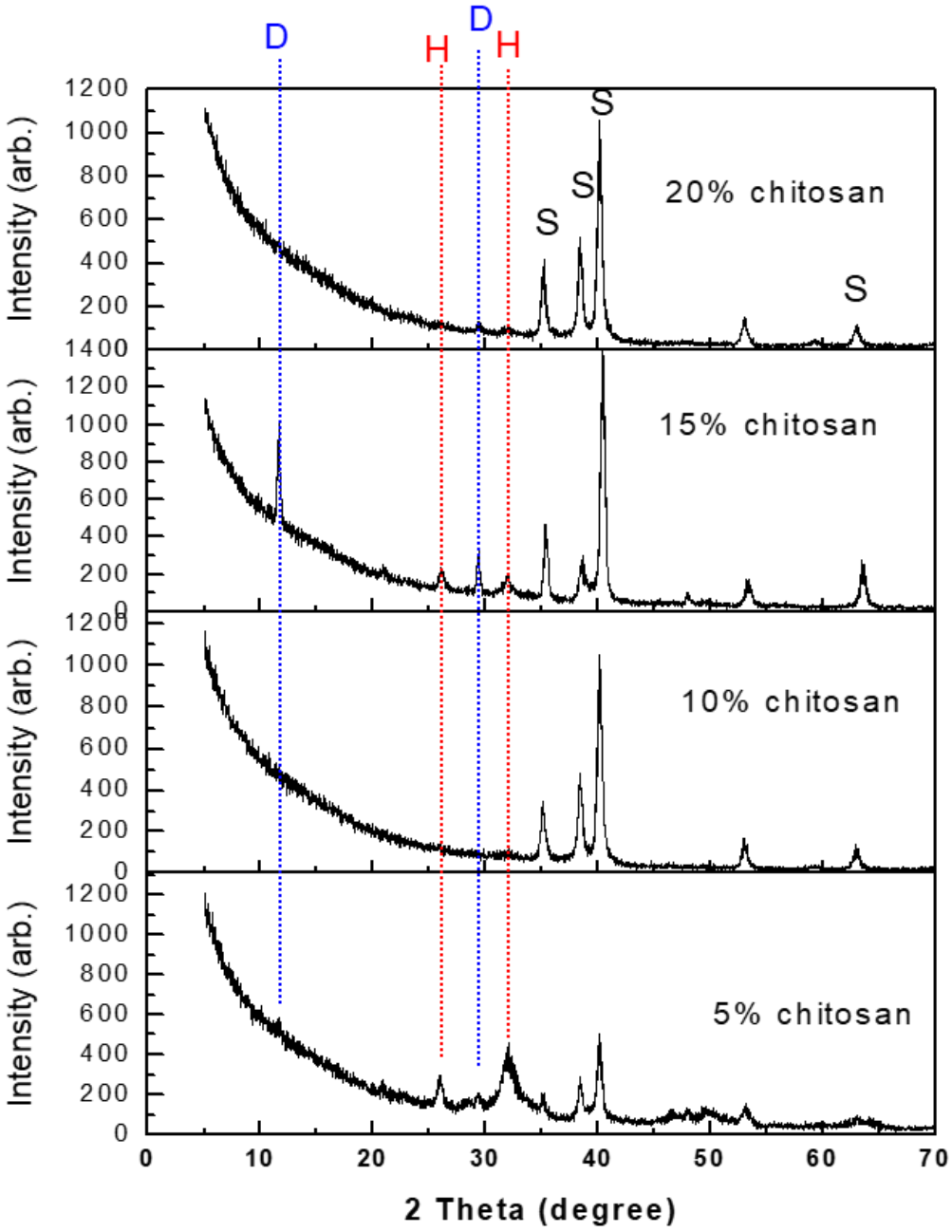

Figure 3. X-ray diffraction of the calcium phosphate-chitosan coating on cp-Ti substrate with different ratios of CaP/CS solution (5 - 20 v/v%). The peaks of dicalcium phosphate dihydrate, hydroxyapatite, and cp-Ti substrate are denoted with D, H, and S, respectively.

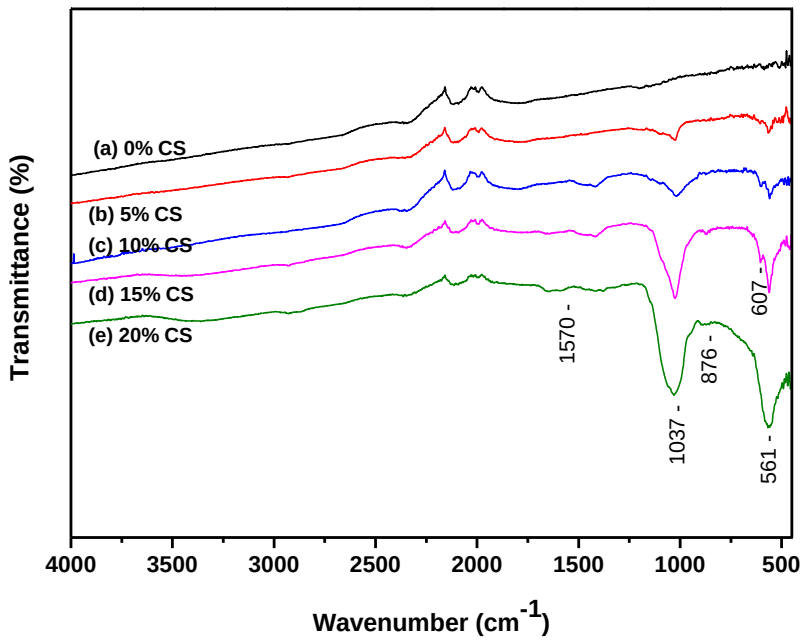

Figure 4. FT-IR spectra of CaP/CS coatings with various chitosan contents.

The Nyquist plots of electrodeposited CaP/CS coating with various contents of CS compared with the cp-Ti substrate are shown in Fig 5. The plot for the CaP/CS coating exhibited a capacitive semicircle at high frequencies, which implied that the coating was undamaged. The diameters of the capacitive semicircles of the CaP/CS coatings were greater than that of the cp-Ti substrate. A dramatic increase in impedance was produced in the CaP/CS coating at 15% CS, which revealed nobler electrochemical behavior of the coatings which delayed ion diffusion and reduced the corrosion rate of the substrate. The CaP/CS coating with 15% CS showed a higher impedance spectrum than the 5%, 10% and 20% CS coatings, and the CaP/CS coating with 5% CS displayed the worst impedance performance. The impedance (Z_{CPE}) of the constant phase elements (CPE) is defined as follows:

$$Z_{CPE} = \frac{1}{Q(jw)^n} \quad (3)$$

In Equation (3), ω denotes the angular frequency, j represents an imaginary number, and n is the slope of impedance versus frequency in the Bode plot. When n is 1, Z_{CPE} is the ideal capacitance. Q_o and Q_i represent the CPEs of the outer layer and inner layer, respectively. The impedance magnitude of the CaP/CS coating at 15% CS is about 13.2 kΩ, which is the highest among all samples (3.5 kΩ at 5% CS, 5.3 kΩ at 10%, and 5.9 kΩ at 20% CS compared with 2.1 kΩ for bare cp-Ti), suggesting that CaP/CS coating significantly improved corrosion resistance compared with bare cp-Ti. This phenomenon may lead to the biological activity of CaP. The impedance spectra using an equivalent circuit model were analyzed for the coating layer/solution interface. The equivalent circuit model assumes that the coating layer on the cp-Ti substrate consists of a barrier-like inner layer and a porous outer layer. These results

are illustrated by fitting the Nyquist plots using the equivalent circuit presented in Fig. 5(b). As listed in Table 1, the CaP/CS coatings exhibit a lower capacitance (Q_o, Q_i) and a higher porous resistance (R_o, R_i) than bare cp-Ti. Low capacitance and high resistance indicate the formation of a highly stable coating on the cp-Ti substrate in the electrolyte. Low capacitance is associated with an increase in the thickness of the passive layer. CaP/CS coating resulted in the formation of a thicker outer porous layer than bare cp-Ti. In particular, the CaP/CS coating containing 15% CS showed a relatively thick passive layer with a capacitance of 13 kΩ, and the outer layers of the other CaP/CS coatings displayed similar properties. The CaP/CS coating with 15% CS in the outer layer resulted in the best corrosion resistance, as shown in Figure 5(a). The fitting results are listed in Table 1.

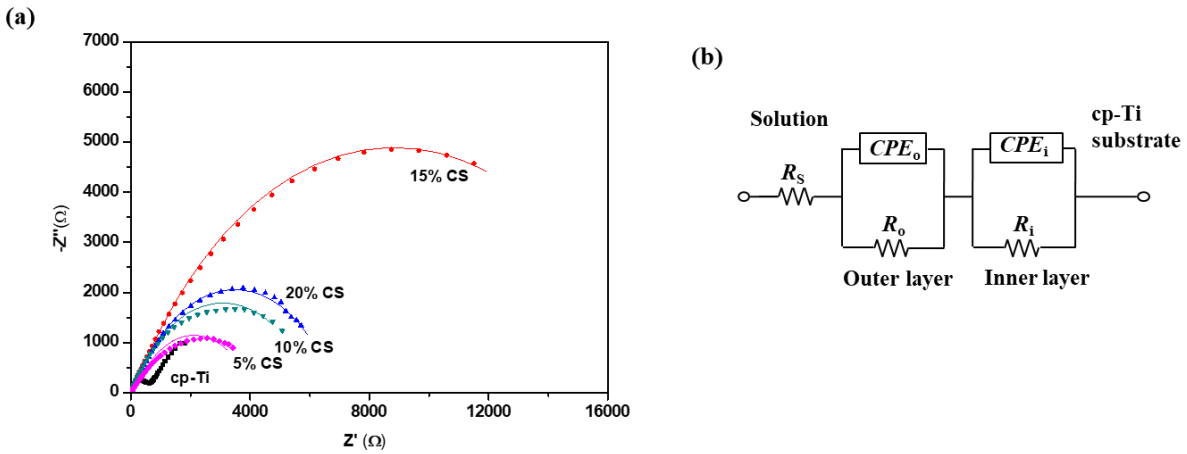

Figure 5. Nyquest plots of CaP/CS coating on cp-Ti formed by pulse electrodeposition at – 5 mA cm^{-2} with various chitosan contents.

Table 1. Impedance parameters of CaP/CS coatings on cp-Ti in 0.9% NaCl solution

Contents of CS	solution	Outer layer			Inner layer			χ^2
	R_S (Ω)	R_o (kΩ)	Q_o (μ S·s^{no})	n_o	R_i (kΩ)	Q_i (μ S·s^{no})	n_i	(×10^{-3})
cp-Ti	13.6	0.58	60.7	0.86	5.42	2650	0.60	0.16
5 %	27.0	4.25	354	0.60	0.50	450	0.25	0.70
10 %	27.7	1.84	165	0.72	3.29	105	0.67	0.12
15 %	30.5	0.82	75.7	0.80	15.9	134	0.81	0.08
20 %	29.2	0.68	132	0.75	6.13	153	0.60	0.10

Fig. 6 presents the potentiodynamic polarization curves of cp-Ti and CaP/CS coatings with different chitosan contents. As shown in Fig. 6, the corrosion potential of the CaP/CS coating was increased and the corrosion current density was lower than that of cp-Ti. The corrosion potential (E_{corr}) is related to the thermodynamic stability of the sample immersed in the electrolyte, whereas the corrosion

current density (I_{corr}) determines the reaction kinetics of corrosion [27].

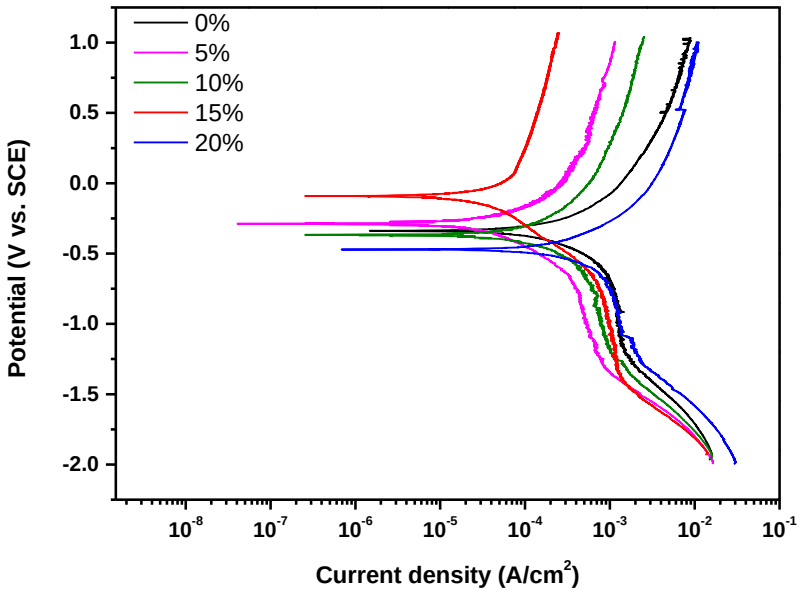

Figure 6. The potentiodynamic polarization curves of CaP/CS coating on cp-Ti formed with various chitosan contents.

Table 2. The corrosion parameters of CaP/CS coatings on cp-Ti in 0.9% NaCl solution

Contents of CS	E_{corr} (V)	I_{corr} (μA cm^{-2})	β_c(mV)	β_a (mV)
cp-Ti	– 0.350	129.88	269	278
5 %	– 0.299	27.35	268	244
10 %	– 0.359	77.13	285	316
15 %	– 0.119	30.67	331	503
20 %	– 0.455	202.13	328	257

Both of these results are attributable to the increased thickness of the CaP/CS coating. The corrosion parameters obtained using fitting software are presented in Table 2. The corrosion potentials (E_{corr} = – 0.299 V and E_{corr} = – 0.359 V) of the CaP/CS coating with 5% CS and 10% CS, respectively, are more positive than those of the CaP/CS coating (E_{corr} = – 0.455 V) containing 20% CS and that of cp-Ti (E_{corr} = – 0.350 V). The most marked increase was observed in the case of CaP/CS coating (E_{corr} = – 0.119 V) with 15% CS. The corrosion current (I_o = 30.67 μA cm^{-2}) of the CaP/CS coating with 15% CS is nearly four-fold lower than that of cp-Ti (I_o = 129.88 μA cm^{-2}). Furthermore, the corrosion current of other samples is two- to three-fold lower than that of bare cp-Ti. The polarization curves of the CaP/CS coating demonstrate lower degradation rates compared with those of cp-Ti, resulting in a decrease in the

active surface for corrosion reactions and the corrosion current density. The polarization results suggest that the CaP/CS coating could improve the corrosion resistance due to the formation of protecting layer on cp-Ti substrate.

4. CONCLUSIONS

PED of CaP/CS coatings on a cp-Ti substrate using an electrolyte solution with various concentrations of chitosan resulted in the formation of DCPD. The CaP/CS coating exhibited an aggregated spindle-like morphology. The XRD patterns and EDS spectra confirmed the formation of DCPD and HA. The CaP/CS coatings showed significant improvement in corrosion resistance because of the presence of protective layers compared with the bare cp-Ti substrate. We expect that the CaP/CS coating prepared via PED represents an appropriate biomaterial for dental implants.

ACKNOWLEDGMENTS
This study was supported by the National Research Foundation of Korea (NRF) grant funded by the Korea government (MSIP) (No. 2017R1A2B1012074 and No. 2019R1A5A2027521).

References

1. J. W. Jeong, J. H. Kim, J. H. Shim, N. S. Hwang, C. Y. Heo, *Biomater. Res.*, 23(1) (2019) 18.
2. M. B. Kannan, O. Wallipa, *Mater. Sci. Eng. C Mater. Biol. Appl.*, 33 (2013) 675.
3. E. Vidal, J. Buxadera-Palomero, C. Pierre, J. M. Manero, M. P. Ginebra, S. Cazalbou, C. Combes, E. Rupérez, D. Rodríguez, *Surf. Coat. Technol.*, 358 (2019) 266.
4. R. A. Surmenev, M. A. Surmeneva, A. A. Ivanova, *Acta Biomater.*, 10 (2014) 557.
5. S. V. Dorozhkin, M. Epple, *Angew Chemie. Int. Ed.*, 41 (2002) 3130.
6. J. Li, B. A. Baker, X. Mou, N. Ren, J. Qiu, R. I. Boughton, H. Liu, *Adv. Healthc. Mater.*, 3(4) (2014) 469.
7. T. Mokabber, Q. Zhou, A. I. Vakis, P. Rijn, Y. T. Pei, *Mater. Sci. Eng. C.*, 100 (2019) 475.
8. T. Hayakawa, M. Kawashita, G. H. Takaoaka, *J. Ceram. Soc. Japan*, 116 (2008) 68.
9. J. Wang, J. de Boer, K. de Groot, *J. Dent. Res.*, 83(4) (2004) 296.
10. N. Eliaz, S. Shmueli, I. Shur, D. Benayahu, D. Aronov, G. Rosenman, *Acta Biomater.*, 5(8) (2009) 3178.
11. T. M. T. Dinh, T. T. Nguyen, T. N. Pham, T. P. Nguyen, T. T. T. Nguyen, T. Hoang, D. Grossin, G. Bertrand, C. Drouet, *Adv. Nat. Sci. Nanosci. Nanotechnol.*, 7 (2016) 025008 (8pp).
12. T. T. Li, L. Ling, M. C. Lin, Q. Jiang, Q. Lin, J. H. Lin, C. W. Lou, *Nanomaterials*, 9(5) (2019) 679.
13. X. Lu, Y. Leng, Q. Zhang, *Surf. Coat. Technol.*, 202(13) (2008) 3142.
14. C. Liu, A. Tian, H. Yang, Q. Xu, X. Xue, *Appl. Surf. Sci.*, 287 (2013) 218.
15. R. Hurteauxe, H. Benhayoune, F. Edwards-Levy, S. Bouthors, G. Balossier, D. Laurent-Maquin, *J Mater. Sci. Mater. Med.*, 16(1) (2005) 9.
16. S. Manara, F. Paolucci, B. Palazzo, M. Marcaccio, E. Foresti, G. Tosi, S. Sabbatini, P. Sabatino, G. Altankov, N. Roveri, *Inorg. Chim. Acta*, 361 (2008) 16345.
17. S. Zhang, X. Cheng, J. Shi, J. Pang, Z. Wang, W. Shi, F. Liu, B. Ji, *Int. J. Electrochem. Sci.*, 13 (2018) 4046.

18. Y. Zhang, M. Zhang, *J. Biomed. Mater. Res.*, 62(3) (2002) 378.
19. K. H. Park, S. J. Kim, M. J. Hwang, H. J. Song, Y. J. Park, *Colloid Polym. Sci*., 295 (2017) 1843.
20. D. Gopi, J. Indira, L. Kavitha, *Surf. Coat. Technol.*, 206 (2012) 2859.
21. D. J. Blackwood, K. H. W. Seah, *Mater. Sci. Eng. C.*, 30 (2010) 561.
22. J. Redepenning, G. Venkataraman, J. Chen, N. Stafford, *J. Biomed. Mater. Res. A.*, 66(2) (2003) 411.
23. M. C. Kuo, S. K. Yen, *Mater. Sci. Eng. C*, 20 (2002) 153.
24. T. K. Anee, M. Palanichamy, M. Ashok, N. M. Sundaram, S. N. Kalkura, *Mater. Lett.*, 58 (2004) 478.
25. N. Shanmugasundaram, P. Ravichandran, P. N. Reddy, N. Ramamurty, S. Pal, K. P. Rao, *Biomaterials*, 22 (2001) 1943.
26. Y.Y. Shi, M. Li, Q. Liu, Z.J. Jia, X.C. Xu, Y. Cheng, Y.F. Zheng, *J. Mater. Sci. Mater. Med.*, 27 (2016) 48.
27. R. Drevet, O. Aaboubi, H. Benhayoune, *J. Solid State Electrochem.*, 16 (2012) 3069.